Assessment of the Orthogonal and Non-Orthogonal Coupled Mode Theory for parallel optical waveguides couplers

GAETANO BELLANCA[1], **PIERO ORLANDI**[2,3], **AND PAOLO BASSI**[2,*]

[1] *Dipartimento di Ingegneria, University of Ferrara, I44122 Ferrara FE, Italy*
[2] *DEI, Alma Mater Studiorum – University of Bologna, Viale del Risorgimento 2 , I40136 Bologna BO, Italy*
[3] *Present address: STMicroelectronics, Via Camillo Olivetti 2, I 20864 Agrate Brianza (MB), Italy*
[*] *Corresponding author: paolo.bassi@unibo.it*

Compiled January 20, 2021

The Coupled Mode Theory (CMT) is a powerful approach routinely used to calculate the effects of spatial mode interactions in perturbed structures, such as optical waveguides. One of its basic hypotheses requires that perturbations are weak. This is usually not the case for devices fabricated with modern semiconductor based technologies. In this paper, the CMT is studied in these critical cases to assess its validity. Attention will be focused on the quite common case of parallel coupled waveguides. For these structures, results can in fact be compared to the exact ones, obtained using super-modes. The study will show that not all the possible expressions of the coupling coefficients are equivalent and which one can be pragmatically used to obtain results with minimum errors with respect to exact solutions.

OCIS codes: *(230.7380) Waveguides, channeled; (130.3120) Integrated optics devices; (230.4555) Coupled resonators; (000.4430) Numerical approximation and analysis.*

http://dx.doi.org/10.1364/josaa.XX.XXXXXX

1. INTRODUCTION

The spatial Coupled Mode Theory (CMT) is a simple and effective approach widely used to model microwave and optical devices where longitudinal structure perturbations induce coupling between the modes propagating along that direction. After its original formulation [1], the CMT has been extended also to optics [2]-[19] to study the electromagnetic behavior of several fundamental devices such as directional couplers, modulators, filters and lasers. More recently, CMT has been also employed to design a wide variety of structures for different applications: multicore optical fibers for spatial division multiplexing [20], non-Hermitian waveguides [21], graphene based devices [22], optical devices with random geometrical variations [23], just to mention some examples.

When it was conceived, the CMT targeted the study of the behavior of two or more parallel cylindrical waveguides or of perturbed structures (e.g. gratings) using the modes of simpler structures (single unperturbed waveguides) instead of those of the actual ones. The possibility to calculate, at least numerically, the solutions of the composite or complex devices was in fact limited by the lack of powerful computational resources. Set up of the theory was based on the fundamental simplifying hypothesis that adding new waveguides or perturbations to the original structure would not significantly alter the characteristics of the modes propagating in each of them. This assumption was consistent with the exploited technologies (i.e. glass fibers and integrated circuits) which allowed low index contrast and largely spaced waveguides. However, since photonic integrated technologies have shifted to larger index contrast (e.g. III-V materials, Germanium, SiN and Silicon On Insulator) also allowing smaller footprints, these assumptions fail. The presence of large perturbations raised then doubts on the CMT applicability. So, many attempts have been done to overcome its intrinsic limits [6]-[19]. The CMT is in fact always attracting since it is simple to be implemented and fast to be run, and then quite interesting when one does not want to use time and computational power hungry numerical techniques (e.g. FDTD, FEM, BPM).

Validation of the various approaches has been however done using only simple structures (2D structures), which are theoretically useful for "proof-of-concept" studies but not when real devices must be designed. In this paper we will then assess the validity of the CMT formulations studying realistic, i.e. 3D, cases taking advantage of the availability of powerful computational tools. The structures we have considered are directional couplers between two parallel waveguides with varying spacing and index contrast. Closely spaced high index contrast structures are typical of modern semiconductor based integrated optical circuits. Couplers with larger spacing and small index contrast describe classical but still used technologies. Parallel waveguide structures have the advantage that allow to compare the CMT results with exact solutions, based on the so called structure super-modes, i.e. the solutions of the whole coupler, which can be calculated numerically. For simplicity, only the case of co-directional coupling between identical waveguides will be considered here. Asymmetrical couplers would in fact introduce a further parameter, the asymmetry degree, which would make result presentation heavier. Counter-directional coupling, generated by gratings, which is another case of interest, will also not be considered. In this case, its assessment would in fact require the explicit knowledge of the super-modes of longitudinally varying structures, which cannot be derived simply (one should use, for example, spatial harmonics [24]) for laterally confined waveguides.

The paper is organized as it follows. The CMT equations will be derived first, highlighting critical points and simplifying assumptions. Then, a co-directional coupler made by two identical parallel isotropic single mode integrated optical waveguides will be considered for the just discussed reasons. Such coupler will be used as a case study to compare the CMT results with the exact ones, which can be obtained using the structure super-modes, as it will be explained. The comparison will consider the effect of varying both the index contrast and the waveguide spacing, ranging from cases in which the CMT approximations do not hold, down to cases where the approximations become realistic. This will show which CMT formulation, among some possible ones, can be heuristically used even when the original simplifying hypotheses fail to be met.

2. THE COUPLED MODE THEORY

In this section the basic equations of the CMT will be derived, starting from the Reciprocity theorem, as in [9]. Since we are interested in assessing a well established theory in a specific case, we will introduce together both the general simplifying assumptions and those related to the case study. This will keep the formal aspect as simple as possible and introduce terminology and symbols necessary to present and discuss the results.

A. Lorentz reciprocity theorem

The Lorentz reciprocity theorem considers two field distributions $\mathbf{E}_1, \mathbf{H}_1$ and $\mathbf{E}_2, \mathbf{H}_2$ as the solutions of Maxwell's equations found in the same volume V with two dielectric media characterized by different dielectric constants ε_1 and ε_2. Maxwell's equations in the two media are then

$$\nabla \times \mathbf{E}_1 = -j\omega\mu\, \mathbf{H}_1 \quad (1)$$

$$\nabla \times \mathbf{H}_1 = j\omega\varepsilon_1\, \mathbf{E}_1 \quad (2)$$

in the former material, while, in the latter, it holds

$$\nabla \times \mathbf{E}_2 = -j\omega\mu\, \mathbf{H}_2 \quad (3)$$

$$\nabla \times \mathbf{H}_2 = j\omega\varepsilon_2\, \mathbf{E}_2. \quad (4)$$

The definition of ε_1 and ε_2 is left to the CMT user. Some possible choices will be discussed in subsection C and relevant results presented in section 4.

Since co-directional coupling will be considered, only the so called *conjugated* form of the reciprocity theorem will be derived. To this purpose, one scalarly premultiplies (1) by $\mathbf{H}_2^*$, (2) by $\mathbf{E}_2^*$, the conjugated of (3) by $\mathbf{H}_1$ and the conjugated of (4) by $\mathbf{E}_1$. The four resulting equations are then reordered also reminding vectorial identities and integrated over the considered cylindrical volume V surrounded by surface S with normal unitary vector $\hat{n}$. After applying the Gauss theorem one finally gets the Lorentz reciprocity theorem basic equation:

$$\int_{S_\infty} \frac{\partial}{\partial z}(\mathbf{E}_1 \times \mathbf{H}_2^* + \mathbf{E}_2^* \times \mathbf{H}_1)\cdot \hat{z}\, dS = -j\omega \int_{S_\infty} \Delta\varepsilon\, \mathbf{E}_1 \cdot \mathbf{E}_2^*\, dS. \quad (5)$$

This equation states that the two field configurations have a mutual effect which depends on the coupling which is generated by the perturbation $\Delta\varepsilon$. The expression of such perturbation will be discussed in subsection C since it depends on the choice of the two media.

The fields to be inserted in these equations are combination of the modes which solve the Maxwell's equations in medium either with ε_1 and with ε_2. In each medium, the transversal components of those fields can then be written as:

$$\mathbf{E}_t(z) = \sum_\nu (a_\nu(z) + b_\nu(z))\, \mathbf{E}_{t\nu}(z) + \int (a_\rho(z) + b_\rho(z))\, \mathbf{E}_{t\rho}(z)\, d\rho \quad (6)$$

$$\mathbf{H}_t(z) = \sum_\nu (a_\nu(z) - b_\nu(z))\, \mathbf{H}_{t\nu}(z) + \int (a_\rho(z) - b_\rho(z))\, \mathbf{H}_{t\rho}(z)\, d\rho \quad (7)$$

with values of a and b different in the two media. The amplitude coefficients of the the incident ($a(z)$) and reflected ($b(z)$) modes, with transversal distribution normalized in power [13], are denoted by an integer subscript ν when they are guided or by a continuous subscript ρ when radiated, since they are a continuum.

B. Simplifying assumptions

The CMT is based on some simplifying assumptions.

i) Radiation modes are neglected, i.e. the integrals in (6) and (7) vanish. This assumption is always reasonable, since structures are designed to minimize power radiation i.e. losses. Reminding that attention is restricted here to co-propagating modes, no reflected fields too will be considered in the following ($b(z) = 0$).

ii) The field shapes in the transversal plane, $\mathbf{E}_{t\nu}(z)$ and $\mathbf{H}_{t\nu}(z)$ are assumed to remain constant along z. Moreover, the amplitude coefficient $a_\nu(z) = A_\nu(z)\, e^{-j\beta_\nu(z)z}$ can be simplified assuming that the mode propagation constants $\beta_\nu(z)$ is longitudinally constant too, letting the z dependence affect only the amplitude coefficients A_ν. These assumptions are reasonable as well, since small structure perturbations should induce also negligible field changes. These positions allow to write (6) and (7) as:

$$\mathbf{E}_t(z) = \sum_\nu a_\nu(z)\, \mathbf{E}_{t\nu} = \sum_\nu A_\nu(z)\, e^{-j\beta_\nu z}\, \mathbf{E}_{t\nu} \quad (8)$$

$$\mathbf{H}_t(z) = \sum_\nu a_\nu(z)\, \mathbf{H}_{t\nu} = \sum_\nu A_\nu(z)\, e^{-j\beta_\nu z}\, \mathbf{H}_{t\nu}. \quad (9)$$

From now on, the explicit mention of z dependence of $A(z)$ and $a(z)$ will be omitted for formal simplicity.

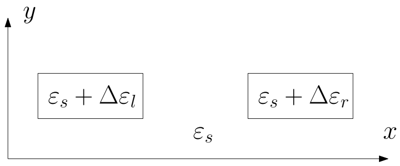

Fig. 1. Schematic of the transversal section of the studied parallel waveguide coupler. The z axis is orthogonal to the design plane; ε_s is the dielectric constant of the structure substrate; $\Delta\varepsilon_l$ and $\Delta\varepsilon_r$ denote the increase of the substrate dielectric constant which constitute the two, left and right, waveguide cores.

iii) The interaction between the two different structures is weak. This requires the right term of (5) to be small. This condition was easily verified when the CMT was conceived, but may not be assumed true nowadays for modern semiconductor based small footprint devices.

One can now include the effects of these simplifying assumptions in (5). To do so, one must preliminarily define the fields "1" and "2" associated to ε_1 and ε_2.

Field "1" is assumed to be a complete set of modes guided by the structure described by ε_1. If so, (6) and (7), reminding also (8) and (9), reduce to:

$$\mathbf{E}_{1t}(z) = \sum_\nu a_\nu \mathbf{E}_{t\nu} \quad (10)$$

$$\mathbf{H}_{1t}(z) = \sum_\nu a_\nu \mathbf{H}_{t\nu}. \quad (11)$$

Field "2" is associated to one of the normalized modes of the structure described by ε_2. It is a "probe" monitoring the power exchange between the two structures:

$$\mathbf{E}_{2t}(z) = \mathbf{E}_{t\mu}\, e^{-j\beta_\mu z} \quad (12)$$

$$\mathbf{H}_{2t}(z) = \mathbf{H}_{t\mu}\, e^{-j\beta_\mu z} \quad (13)$$

where μ denotes the mode that is considered among those guided by structure "2".

Substituting (10-11) and (12-13) into (5), its left hand side integral becomes then:

$$\int_{S_\infty} \frac{\partial}{\partial z} \left[\sum_\nu a_\nu \mathbf{E}_{t\nu} \times \mathbf{H}^*_{t\mu}\, e^{j\beta_\mu z} + \mathbf{E}^*_{t\mu}\, e^{j\beta_\mu z} \times \sum_\nu a_\nu \mathbf{H}_{t\nu} \right] \cdot \hat{\mathbf{z}}\, dS. \quad (14)$$

Nothing has been said so far on the structures ε_1 and ε_2 associated to the fields with suffixes "1" and "2". This becomes mandatory when the right term of (5) must be expressed, since the perturbation $\Delta\varepsilon$ has not yet been be defined. This will be done in the next section.

C. The coupling coefficient

As said in the previous section, and pointed out also, for example, in [15], different choices of ε_1 and ε_2 are possible. Two of them will be introduced and discussed, considering the device which is investigated: a coupler made by two equal parallel waveguides. A sketch of the device is shown in figure 1. The substrate relative dielectric constant is ε_s, while $\Delta\varepsilon_l$ and $\Delta\varepsilon_r$ describe the changes due to the two left and right waveguide cores. Suffix l and r are used only to identify the waveguide, since, in the present case, $\Delta\varepsilon_l = \Delta\varepsilon_r = \Delta\varepsilon$.

C.1. First choice of the dielectric constants

As a first choice, one can consider, following the perturbation approach used in [3], medium "1" as the coupler made by the two waveguides, with dielectric constant $\varepsilon_1 = \varepsilon_s + \Delta\varepsilon_l + \Delta\varepsilon_r$ and medium "2" as one of its two waveguides, for example the right one, i.e. $\varepsilon_2 = \varepsilon_s + \Delta\varepsilon_r$. Field "1" field is then a linear combination of the so called super-modes of the full structure, while field "2" is any mode, one at a time, of the right waveguide.

The final expression of the right term of (5) was found using the simplifying assumption *iii)* which allows to write the super-modes of the coupler, which were difficult to be calculated when the CMT was conceived, as a linear combination of the modes of the left and right single waveguides and supposing also that the two sets of modes are mutually orthogonal. This is not true in general, but can be assumed approximately true when the index contrast is small or the waveguides are not close each other, so that they can be considered weakly coupled and their modes independent. Always following [3], the right term of (5) reduces then to:

$$-j4 \sum_\nu \kappa\, A_\nu\, e^{-j(\beta_\nu - \beta_\mu)z} \quad (15)$$

where the coupling coefficient κ has been introduced to describe the mode interaction strength. Since orthogonality holds only for the transversal field components, longitudinal and transversal fields had to be managed separately and the overall coupling coefficient resulted, [3], as the sum of $\kappa^t_{\nu\mu}$ and $\kappa^z_{\nu\mu}$, respectively the *transverse* and *longitudinal coupling coefficients*, defined as:

$$\kappa^t_{\nu\mu} = \frac{\omega}{4} \int_{S_{\Delta\varepsilon}} \Delta\varepsilon\, \mathbf{E}_{t\nu} \cdot \mathbf{E}^*_{t\mu}\, dS \quad (16)$$

$$\kappa^z_{\nu\mu} = \frac{\omega}{4} \int_{S_{\Delta\varepsilon}} \frac{\varepsilon\, \Delta\varepsilon}{\varepsilon + \Delta\varepsilon} E_{z\nu}\, E^*_{z\mu}\, dS \quad (17)$$

where $\varepsilon = \varepsilon_s + \Delta\varepsilon_l + \Delta\varepsilon_r$, $\Delta\varepsilon = \Delta\varepsilon_r$ and the integral is evaluated only in the region $S_{\Delta\varepsilon}$ where $\Delta\varepsilon \neq 0$.

As one can see, the transversal and longitudinal components are then differently weighted in the expression of κ.

Moreover, when the CMT was conceived, $\Delta\varepsilon$ was small and the longitudinal field components too were then small. The longitudinal coupling coefficient could then be neglected without problems. As mentioned before, this is however no longer true today for high index contrast waveguides.

Though effective in solving the problem, this approach uses, at least in the intermediate steps, the structure super-modes. In the next subsection a different approach will be illustrated, which does not use them.

C.2. Second choice of the dielectric constants

A second possible choice of the two media associates suffix "1" to one of the two waveguides, and suffix "2" to the other. Always with reference to figure 1, medium "1" is then the left waveguide of the coupler, with dielectric constant $\varepsilon_1 = \varepsilon_s + \Delta\varepsilon_l$ while medium "2" is the right waveguide, with $\varepsilon_2 = \varepsilon_s + \Delta\varepsilon_r$. Field "1" is then a linear combination of the modes of the left waveguide, while field "2" is any mode, one at a time, of the right waveguide.

Also the definition of perturbation, i.e. what should be added to each waveguide to obtain the complete structure, is easier here. For example, $\Delta\varepsilon_r$ is the perturbation to be added to the left waveguide $\varepsilon_s + \Delta\varepsilon_l$ to obtain the complete coupler structure $\varepsilon_s + \Delta\varepsilon_l + \Delta\varepsilon_r$.

In this case, one can easily find that the transversal coupling coefficient $\kappa^t_{\nu\mu}$ is given again by (16), while the longitudinal coupling coefficient turns out to be:

$$\kappa^z_{\nu\mu} = \frac{\omega}{4}\int_{S_{\Delta\varepsilon}} \Delta\varepsilon\, E_{z\nu}\, E^*_{z\mu}\, dS. \tag{18}$$

In both (16) and (18) $\Delta\varepsilon = \Delta\varepsilon_r$.

A further advantage given by this second choice is that supermodes are not invoked and there is then no need to decompose them into a linear combination of the modes of the two structures and suppose that the two sets are orthogonal. This makes assumption *iii)* less important in the CMT.

One can also observe that, if $\Delta\varepsilon \ll \varepsilon$, the expression of the longitudinal coupling coefficient $\kappa^z_{\nu\mu}$ given by (17) simplifies into (18). This has been often done (see, for example, [3]) but does not hold for high index contrast waveguides. Using this approach, (18) is exact. This makes the two approaches independent.

The impact of these assumptions and choices on the CMT will be discussed in the next section.

D. The coupled mode equations

It is now time to derive the CMT equations. This can be done in two ways. The former assumes the modes of the two separate structures as mutually orthogonal. It is the original one and leads to the so called *Orthogonal CMT* (O-CMT) [2–7]. The latter was proposed when failure of the simplifying hypotheses could no longer be neglected and is known as *Non Orthogonal CMT* (NO-CMT) [8, 9, 11].

D.1. Orthogonal CMT

If the two sets of guided modes are assumed to be orthogonal, the left term of (5) can be written

$$\int_{S_\infty} \mathbf{E}_{t\nu} \times \mathbf{H}^*_{t\mu} \cdot \hat{\mathbf{z}}\, dS = 2P\delta_{\nu\mu} \tag{19}$$

$$\int_{S_\infty} \mathbf{E}^*_{t\mu} \times \mathbf{H}_{t\nu} \cdot \hat{\mathbf{z}}\, dS = 2P\delta_{\mu\nu} \tag{20}$$

where $\delta_{\mu\nu}$ is the Kronecker symbol ($= 1$ if $\mu = \nu$, $= 0$ if $\mu \neq \nu$) and $P\delta_{\mu\mu}$ is then the power of the μ-*th* mode. Since $\delta_{\nu\mu} = \delta_{\mu\nu}$, (14) reduces to:

$$\int_{S_\infty} \frac{\partial}{\partial z}\left[a_\mu\, \mathbf{E}_{t\mu} \times \mathbf{H}^*_{t\mu}\, e^{j\beta_\mu z} + \mathbf{E}^*_{t\mu}\, e^{j\beta_\mu z} \times a_\mu\, \mathbf{H}_{t\mu}\right] \cdot \hat{\mathbf{z}}\, dS =$$

$$= 4P\frac{\partial A_\mu}{\partial z}. \tag{21}$$

Normalizing mode powers to 1 and inserting (15) into the right term of (5), one finally gets the *Coupled Mode Equations* valid for the O-CMT:

$$\frac{\partial A_\mu}{\partial z} = -j\sum_\nu \left[A_\nu \left(\kappa^t_{\nu\mu} + \kappa^z_{\nu\mu}\right) e^{-j(\beta_\nu-\beta_\mu)z}\right]. \tag{22}$$

In the case of a coupler made by two parallel single mode guides, with propagation along the positive direction of z, the only possible values for both ν and μ are 1 and 2. Suffix 1 refers to the mode of the left waveguide, while suffix 2 refers to the right one. Introducing the explicit values of ν and μ one gets:

$$\frac{\partial A_1}{\partial z} = -jA_1\left(\kappa^t_{11} + \kappa^z_{11}\right) - jA_2\left(\kappa^t_{21} + \kappa^z_{21}\right) e^{-j(\beta_2-\beta_1)z} \tag{23}$$

$$\frac{\partial A_2}{\partial z} = -jA_1\left(\kappa^t_{12} + \kappa^z_{12}\right) e^{-j(\beta_1-\beta_2)z} - jA_2\left(\kappa^t_{22} + \kappa^z_{22}\right). \tag{24}$$

The self coupling coefficients κ_{ii} are usually neglected, since they are assumed to be higher order infinitesimals [3].

D.2. Non Orthogonal CMT

If modes cannot be considered orthogonal, integrals in (19-20) never vanish and one must write:

$$\int_{S_\infty} \mathbf{E}_{t\nu} \times \mathbf{H}^*_{t\mu} \cdot \hat{\mathbf{z}}\, dS = 2P'_{\nu\mu} \tag{25}$$

and

$$\int_{S_\infty} \mathbf{E}^*_{t\mu} \times \mathbf{H}_{t\nu} \cdot \hat{\mathbf{z}}\, dS = 2P'_{\mu\nu}. \tag{26}$$

Letting $4P_{\nu\mu} = 2P'_{\nu\mu} + 2P'_{\mu\nu}$, the right term of (14) becomes then:

$$4\sum_\nu \left[\left(\frac{\partial A_\nu}{\partial z} - j(\beta_\nu - \beta_\mu)\, A_\nu\right) e^{-j(\beta_\nu-\beta_\mu)z}\, P_{\nu\mu}\right]. \tag{27}$$

The NO-CMT equations to be solved are then:

$$\sum_\nu \left(\frac{\partial A_\nu}{\partial z} - j(\beta_\nu - \beta_\mu)\, A_\nu\right) e^{-j(\beta_\nu-\beta_\mu)z}\, P_{\nu\mu} =$$

$$= -j\sum_\nu A_\nu\, e^{-j(\beta_\nu-\beta_\mu)z}\left(\kappa^t_{\nu\mu} + \kappa^z_{\nu\mu}\right). \tag{28}$$

Considering two single mode waveguides with modes propagating along the positive direction of z, (28) becomes:

$$\frac{\partial A_1}{\partial z} P_{11} + \left(\frac{\partial A_2}{\partial z} - j(\beta_2 - \beta_1)\, A_2\right) e^{-j(\beta_2-\beta_1)z}\, P_{21} =$$

$$= -jA_1\,\kappa_{11} - jA_2 e^{-j(\beta_2-\beta_1)z}\,\kappa_{21} \tag{29}$$

$$\left(\frac{\partial A_1}{\partial z} - j(\beta_1 - \beta_2)\, A_1\right) e^{-j(\beta_1-\beta_2)z}\, P_{12} + \frac{\partial A_2}{\partial z} P_{22} =$$

$$= -jA_1\, e^{-j(\beta_1-\beta_2)z}\,\kappa_{12} - jA_2\,\kappa_{22}. \tag{30}$$

Multiplying (29) by $e^{-j\beta_1 z}$ and (30) by $e^{-j\beta_2 z}$ and rearranging in matrix form, one gets:

$$\begin{bmatrix} P_{11}\, e^{-j\beta_1 z} & P_{21}\, e^{-j\beta_2 z} \\ P_{12}\, e^{-j\beta_1 z} & P_{22}\, e^{-j\beta_2 z} \end{bmatrix} \frac{\partial}{\partial z} \begin{bmatrix} A_1 \\ A_2 \end{bmatrix} = \begin{bmatrix} -j\kappa_{11}\, e^{-j\beta_1 z} & j\left[P_{21}\left(\beta_2 - \beta_1\right) - \kappa_{21}\right] e^{-j\beta_2 z} \\ j\left[P_{12}\left(\beta_1 - \beta_2\right) - \kappa_{12}\right] e^{-j\beta_1 z} & -j\kappa_{22}\, e^{-j\beta_2 z} \end{bmatrix} \begin{bmatrix} A_1 \\ A_2 \end{bmatrix}$$

which, after simple algebra, becomes:

$$\frac{\partial}{\partial z}\begin{bmatrix} A_1 \\ A_2 \end{bmatrix} = \frac{1}{P_{11}\, P_{22} - P_{12}\, P_{21}} \begin{bmatrix} P_{22}\, e^{j\beta_1 z} & -P_{21}\, e^{j\beta_1 z} \\ -P_{12}\, e^{j\beta_2 z} & P_{11}\, e^{j\beta_2 z} \end{bmatrix} \begin{bmatrix} -j\kappa_{11}\, e^{-j\beta_1 z} & j\left[P_{21}\left(\beta_2 - \beta_1\right) - \kappa_{21}\right] e^{-j\beta_2 z} \\ j\left[P_{12}\left(\beta_1 - \beta_2\right) - \kappa_{12}\right] e^{-j\beta_1 z} & -j\kappa_{22}\, e^{-j\beta_2 z} \end{bmatrix} \begin{bmatrix} A_1 \\ A_2 \end{bmatrix}.$$

This system can be finally written:

$$\frac{\partial}{\partial z}\begin{bmatrix} A_1 \\ A_2 \end{bmatrix} = -j\begin{bmatrix} \tilde{\kappa}_{11} & \tilde{\kappa}_{21}\, e^{j(\beta_1-\beta_2)z} \\ \tilde{\kappa}_{12}\, e^{-j(\beta_1-\beta_2)z} & \tilde{\kappa}_{22} \end{bmatrix}\begin{bmatrix} A_1 \\ A_2 \end{bmatrix} \quad (31)$$

with the NO-CMT self-coupling coefficients $\tilde{\kappa}_{11}$ and $\tilde{\kappa}_{22}$ and mutual coupling coefficients $\tilde{\kappa}_{12}$ and $\tilde{\kappa}_{21}$ given by:

$$\tilde{\kappa}_{11} = \frac{P_{22}\,\kappa_{11} - P_{21}\,\kappa_{12} + P_{21}\,P_{12}\,(\beta_1-\beta_2)}{P_{11}\,P_{22} - P_{12}\,P_{21}} \quad (32)$$

$$\tilde{\kappa}_{21} = \frac{P_{22}\,\kappa_{21} - P_{21}\,\kappa_{22} - P_{22}\,P_{21}\,(\beta_2-\beta_1)}{P_{11}\,P_{22} - P_{12}\,P_{21}} \quad (33)$$

$$\tilde{\kappa}_{12} = \frac{P_{11}\,\kappa_{12} - P_{12}\,\kappa_{11} - P_{11}\,P_{12}\,(\beta_1-\beta_2)}{P_{11}\,P_{22} - P_{12}\,P_{21}} \quad (34)$$

$$\tilde{\kappa}_{22} = \frac{P_{11}\,\kappa_{22} - P_{12}\,\kappa_{21} + P_{12}\,P_{21}\,(\beta_2-\beta_1)}{P_{11}\,P_{22} - P_{12}\,P_{21}}. \quad (35)$$

When, as in the considered case, the two waveguides have the same size, equations (32-35) simplify since $\beta_1 = \beta_2$ and $P_{12} = P_{21}$, getting $\tilde{\kappa}_{11} = \tilde{\kappa}_{22}$ and $\tilde{\kappa} = \tilde{\kappa}_{12} = \tilde{\kappa}_{21}$. $P_{11} = P_{22} = 1$ are the normalized powers carried by the modes of the single waveguides.

3. THE CASE STUDY: CO-DIRECTIONAL COUPLING OF SINGLE MODE WAVEGUIDES

In this section, the values of the coupling coefficients calculated with different degree of approximation will be compared with the exact solutions, derived from the coupler super-modes propagation constants calculated by means of a commercial mode solver, COMSOL [25]. This software is used to calculate, using the Finite Element Method, both the modes of the single (left and right) waveguides and those of the overall structure (the super-modes) with the relevant propagation constants.

The value of the coupling coefficient resulting from super-modes, which will be considered as the exact, reference, solution, can be calculated observing that power transfer between adjacent waveguides, described by the CMT as a mode coupling effect between the modes of the single waveguides, comes in reality from the interference between the structure super-modes. They propagate with close but different propagation constants and then mutually interfere (see, for example, [26]). Limiting attention to the two lowest order modes of a coupler, exhibiting even and odd symmetries, interference mimics then complete power transfer between the two waveguides at the so-called coupling length L_c given by

$$L_c = \frac{\pi}{\Delta\beta} \quad (36)$$

where $\Delta\beta$ is the difference of the propagation constants of the two super-modes.

With this approach, the coupling coefficient κ, is related to the coupling length (see, for example, [27]) by

$$L_c = \frac{\pi}{2\kappa}. \quad (37)$$

Combining (36) and (37), the exact value of the coupling coefficient as a function of the super-mode propagation constants difference turns out to be:

$$\kappa = \frac{\Delta\beta}{2}. \quad (38)$$

This value will be compared with the results of the different expressions of the coupling coefficients obtained numerically evaluating the integrals (16-18) using the fields computed with COMSOL. In particular, three possible values of the coupling coefficient κ will be considered for the O-CMT:

i) the transverse coupling coefficient alone, i.e. $\kappa = \kappa_t$, as given by (16), which does not depend on the dielectric constant choice discussed in section 2.C;

ii) $\kappa = \kappa_t + \kappa_{za}$ with the dielectric constant distribution illustrated in section 2.C.1, so that κ_t is given by (16) and κ_{za} is given by (17). This result comes also using the perturbation approach to derive the CMT proposed in [3];

iii) $\kappa = \kappa_t + \kappa_{zb}$ with the dielectric constant distribution illustrated in section 2.C.2, so that: κ_t is always given by (16) and κ_{zb} is given by (18).

In the case of the NO-CMT, the following expressions of $\tilde{\kappa}$ will be evaluated and compared:

i) $\tilde{\kappa} = \tilde{\kappa}_t$

ii) $\tilde{\kappa} = \tilde{\kappa}_t + \tilde{\kappa}_{za}$

iii) $\tilde{\kappa} = \tilde{\kappa}_t + \tilde{\kappa}_{zb}$.

They correspond to the previous ones, but use (34) to evaluate the transversal and longitudinal coupling coefficients.

4. RESULTS

To assess the O-CMT and the NO-CMT, some case studies based on 3D structures with different (large, average medium) index contrast to mimic various technological possibilities will be considered. This investigation will allow a general assessment of the different approaches of the CMT theory in all the possible practical cases.

A. Large index contrast coupler

The firs case study considers a SOI coupler formed by two single-mode Silicon waveguides each with a 480×220 *nm* size, embedded in a Silica substrate [28, 29] operated at $\lambda = 1550$ *nm*. This case is particularly interesting since it refers to a widely used technology with very high index contrast waveguides. Coupler features will then be varied to analyze the effect of the structure parameters on the O-CMT and NO-CMT coupling coefficients compared to those obtained evaluating the beating length of the coupler super-modes. As said before, the two coupler waveguides are assumed to be identical and supporting only the first *quasi-TE* and *quasi-TM* modes to reduce the number of parameters to be varied in the comparison. These do not look too limiting assumptions, since monomodality and mode synchronism are often required as operating conditions. Figures 2 and 3 show the E_x and the E_z components of the *quasi-TE* mode and the E_y and the E_z components of the *quasi-TM* mode respectively. The ratio between the maximum value of the modulus of E_z and that of the major transversal component is respectively about 0.5 and 0.6 for the two polarizations. The right waveguide, shown in the figure for a gap of 200 *nm*, is not present in the studied structure but is anyway sketched for visual aid to illustrate its position in the waveguide coupler and appreciate better its interaction with the evanescent field tail of the other waveguide.

The coupler has a minimum gap of 200 *nm*, chosen according to technological constraints [28, 29]. We assume a maximum gap of 500 nm to limit the circuit footprint. The components of the *quasi-TE* and the *quasi-TM* coupler super-modes are shown in Figures 4 and 5 respectively (always for the minimum value of the gap). A strong interaction between the guides exists.

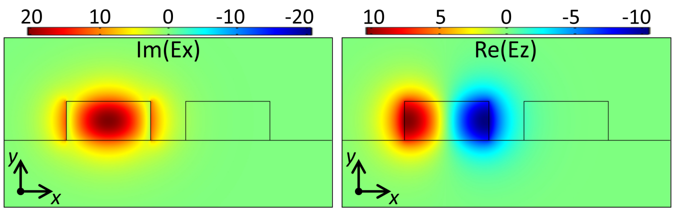

Fig. 2. Imaginary part of E_x (left) and real part of E_z (right) of the *quasi-TE* mode of the left high index contrast waveguide (480 × 220 nm size) alone. The right waveguide, separated by a 200 nm gap, is not present in the studied structure but is anyway sketched for visual aid as explained in the text. The ratio between the maximum value of the moduli of E_z and E_x is about 0.5. (Color online).

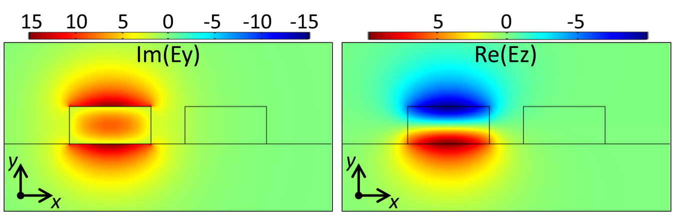

Fig. 3. Imaginary part of E_y (left) and real part of E_z (right) of the *quasi-TM* mode of left high index contrast waveguide (480 × 220 nm size) alone. The right waveguide is not present in the studied structure but is anyway sketched for visual aid as explained in the text. The ratio between the maximum value of the moduli of E_z and E_y is about 0.6. (Color online).

Figure 6 shows the values of the O-CMT coupling coefficient vs the gap in the *quasi-TE* case. The long-dashed black line shows values of κ obtained using (38) and can then be assumed as the exact solution to be compared to the CMT results. The red solid line shows $\kappa = \kappa_t$, the blue dashed line shows $\kappa = \kappa_t + \kappa_{za}$, while the dashed green line, practically superimposed by the black one, shows $\kappa = \kappa_t + \kappa_{zb}$. Both $\kappa = \kappa_t$ and $\kappa = \kappa_t + \kappa_{za}$ strongly differ from (38), while an almost perfect overlap exists between the expected results and the CMT ones using the $\kappa = \kappa_t + \kappa_{zb}$. Results obtained with the NO-CMT differ from those obtained using the O-CMT only about 1% for the gap of 200 nm down to almost 0% for the gap of 500 nm (the curves that mutually differ more are those based on (18); those who differ less are those with (16)). In this case, there is then no practical difference between the O-CMT and the NO-CMT results, which makes useless the extra computational burden necessary to evaluate (34).

Figure 7 shows the same results in the *quasi-TM* case. Again the O-CMT and the NO-CMT produce quite similar results. Differences between the corresponding O-CMT and NO-CMT curves range from about 1% for the gap of 200 nm down to about 0.2% for the gap of 500 nm. Again, curves with differ more are those based on (18); those who differ less are those with (16).

For larger gaps, the coupling coefficient curves are closer than those of the *quasi-TE* case since E_y decays less in the transversal direction, causing larger κ_t and smaller percent contribution of

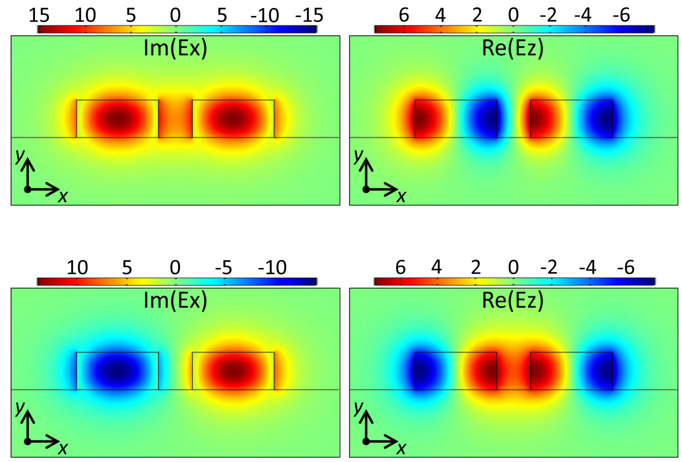

Fig. 4. Imaginary part of E_x (left) and real part of E_z (right) of the two *quasi-TE* super-modes of the high index contrast coupler with even (upper line) and ower line) symmetries. Waveguides have 480 × 220 nm size with a 200 nm gap. In both cases, the ratio between the maximum value of the moduli of E_z and E_x is about 0.5 (Color online).

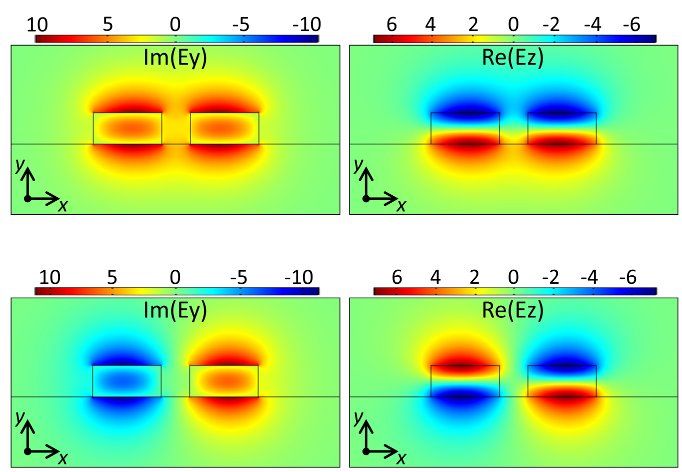

Fig. 5. Imaginary part of E_y (left) and real part of E_z (right) of the two *quasi-TM* super-modes of the high index contrast coupler with even (upper line) and odd (lower line) symmetries. Waveguides have 480 × 220 nm size with a 200 nm gap. In both cases, the ratio between the maximum value of the moduli of E_z and E_x is about 0.6. (Color online).

E_z. The interaction strength changes, but the conclusions on the curve relationships do not: the best results still come using (18).

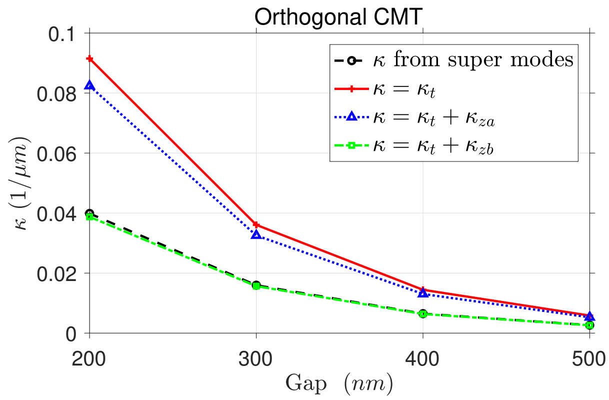

Fig. 6. Coupling coefficient κ vs waveguide gap for the *quasi-TE* mode of a Si waveguide obtained with the O-CMT. The black long dashed line with open circles comes using (38). The red solid line with crosses shows κ_t. The blue dashed-dotted with triangles lined shows $\kappa_t + \kappa_{za}$. The green dashed dotted line with squares (almost superimposed to the black long dashed line) shows $\kappa_t + \kappa_{zb}$. (Color online).

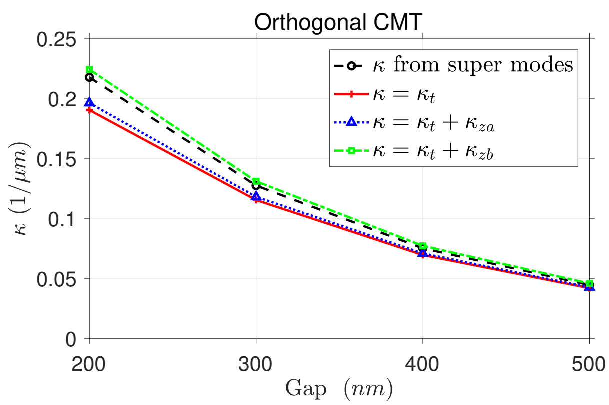

Fig. 7. Coupling coefficient κ vs waveguide gap for the *quasi-TM* mode of a Si waveguide with the O-CMT. Line types as in Figure 6. (Color online).

These results demonstrate that the choice of the expression of the coupling coefficient κ is a critical issue for large index contrast. In particular, the longitudinal component contribution cannot be neglected and the best results are obtained using $\kappa = \kappa_t + \kappa_{zb}$. Values of κ computed with the different expressions tend however to converge for increasing values of the gap, as expected since waveguides have smaller interactions.

It can also be noticed that there is a strong polarization dependence of the CMT results.

B. Average index contrast coupler

The second studied case considers a coupler with the same geometrical features but reduced index contrast $\Delta\varepsilon$. The substrate refractive index value was then increased to 2.2. The modulus of the longitudinal component of the electric field is now about 0.4 and 0.5 the modulus of the major transversal one for the *quasi-TE* and *quasi-TM* modes respectively.

Results for the *quasi-TE* and *quasi-TM* modes coupling coefficients vs gap are reported in Figures 8 and 9 respectively. Only the O-CMT curves are shown in the two figures, since the NO-CMT results are also in this case undistinguishable from them. For the *quasi-TE* case, differences between the O-CMT and NO-CMT curves range from less than 1% for the gap of 200 *nm* down to almost 0% for the gap of 500 *nm*. For the *quasi-TM* case, differences between the curves range from about 1.2% for the gap of 200 *nm* down to about 0.2% for the gap of 500 *nm*. Again, in both cases, curves that differ more are those based on (18); those who differ less are those with (16).

Comparing these results with those of the high contrast waveguide, one can observe that the coupling coefficients increase for the *quasi-TE* mode and decrease for the *quasi-TM* one, i.e. the polarization dependence of coupling decreases. This is the overall effect of the changes of the field components which are less confined and vary their relative weight. This trend will be confirmed and commented studying low contrast waveguides.

Moreover, since κ_{za} and κ_{zb} are smaller, separation among the three CMT coefficient curves decreases. In any case, the general results obtained for the high index contrast structure are confirmed: the curve of κ as a function of the gap obtained with $\kappa = \kappa_t + \kappa_{zb}$ almost exactly superimposes again to that obtained using the super-modes.

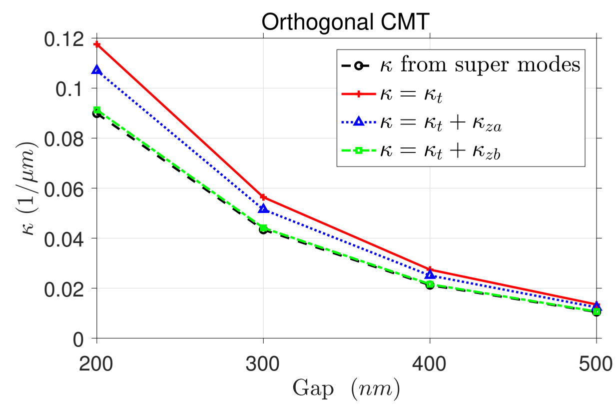

Fig. 8. Coupling coefficient κ vs waveguide gap for the *quasi-TE* mode of the average index contrast waveguide obtained using O-CMT. Line types as in Figure 6. (Color online).

C. Low index contrast coupler

In the last case, the substrate refractive index was further increased to 3, creating an even smaller index contrast coupler. The dielectric constant contrast is anyway not small enough to guarantee waveguides independence and then super-mode complete degeneracy. Figure 10 shows in fact the values of the effective indexes (n_{eff}) of the two *quasi-TE* super-modes (red solid line) and those of the two *quasi-TM* super-modes (blue dashed line) vs gap. Curves are well separated, confirming the not negligible waveguide interaction: values of n_{eff} of the *quasi-TE* and *quasi-TM* mode pairs would in fact be almost degenerate for independent guides.

In this case the maximum modulus of the longitudinal component of the electric field reduces to about 1/4 of that of the transversal one for both polarizations. This and the small dielectric contrast make almost vanish the contribution of the field longitudinal components to κ: curves showing the three different values of κ are in fact almost superimposed. This is shown

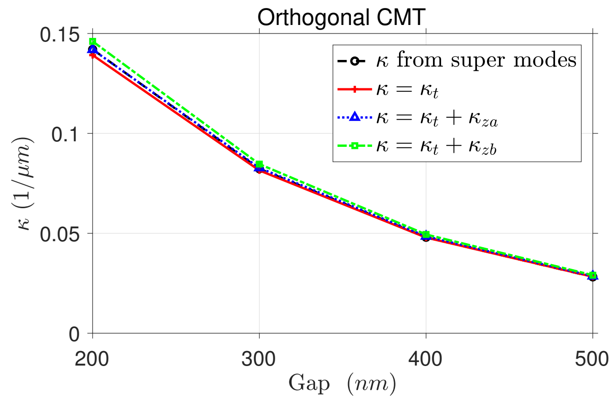

Fig. 9. Coupling coefficient κ vs waveguide gap for the *quasi-TM* mode of the average index contrast waveguide obtained using O-CMT. Line types as in Figure 6. (Color online).

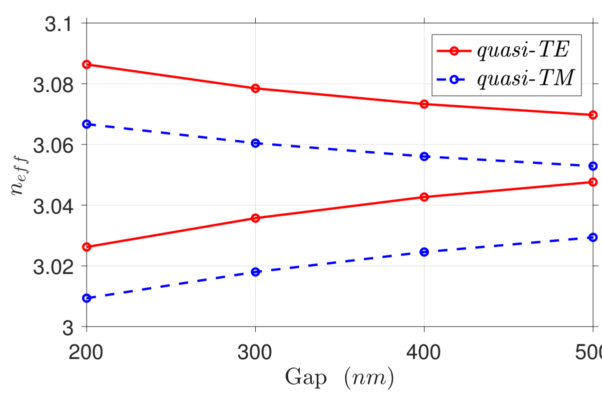

Fig. 10. Effective indexes of the *quasi-TE* and *quasi-TM* modes vs gap. Red solid lines refer to the two *quasi-TE* polarized super-modes, blue dashed lines refer to the *quasi-TM* polarized super-modes. (Color online).

in figures 11 and 12 for the *quasi-TE* and *quasi-TM* modes respectively. In these figures one can also notice that the bundle of the curves with the O-CMT results tend to be closer to the super-mode results than the NO-CMT ones. Paradoxically, it seems that the NO-CMT has worse performance in this case.

Finally, comparing these and the preceding figures, one can observe that, for decreasing index contrast, *quasi-TE* and *quasi-TM* coupling coefficients are more and more similar. In this case they are not yet equal, confirming that full degeneracy of the super modes has not yet been reached. A further increase of the substrate refractive index should then make the results fully superimposed, reaching the polarization insensitivity assumed by the original formulation.

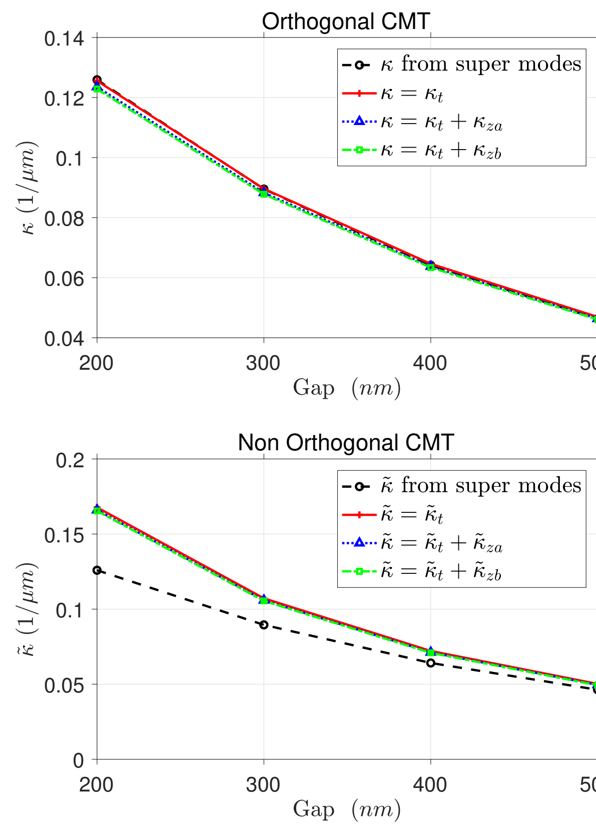

Fig. 11. Coupling coefficient κ vs waveguide gap for the *quasi-TE* mode of the low index contrast waveguide. Top: O-CMT; bottom: NO-CMT. Line types as in Figure 6. (Color online).

5. CONCLUSIONS

In this paper the Coupling Mode Theory (CMT) has been studied to assess its validity in the case of co-directional coupling for two parallel and equal waveguides with different index contrasts and different gaps. Realistic 3D structures have been considered. Tests have been made both for the *quasi-TE* and the *quasi-TM* polarizations to highlight the effects of failure of the CMT basic simplifying assumptions in the considered devices. Both Orthogonal and Non Orthogonal CMT equations have been used. Only equal coupled waveguides have been considered, to avoid the introduction of a parameter related to guide asymmetry, which would have complicated presentation and discussion of the results. Grating induced coupling, which is a practically important case as well, could not be considered in this study since there is no easily evaluable solution for structures with gratings.

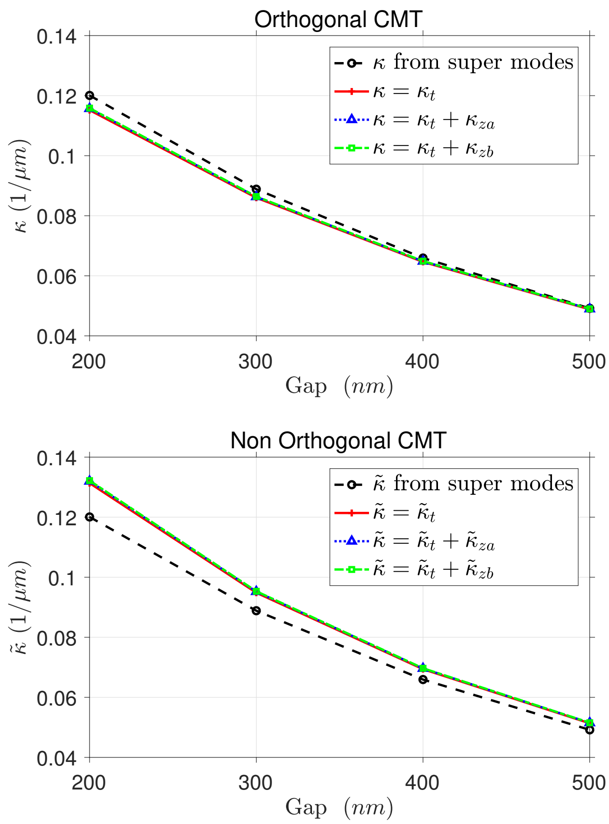

Fig. 12. Coupling coefficient κ vs waveguide gap for the *quasi-TM* mode of the low index contrast waveguide. Top: O-CMT; bottom: NO-CMT. Line types as in Figure 6. (Color online).

Comparisons between the results obtained with CMT, considering both Orthogonal and Non Orthogonal approaches, and those of the exact approach, based on the waveguide supermode solutions for varying refractive indices and waveguide separation, have shown that: *i)* considering mode non orthogonality does not improve result precision; *ii)* the longitudinal coupling coefficient should be included to obtain better results; *iii)* the choice of the dielectric constant decomposition necessary to identify the two coupled structures is important. In particular, the best results come if the coupling coefficient is computed as $\kappa = \kappa_t + \kappa_{zb}$, i.e. including the contribution of the longitudinal field components weighted only by the dielectric constant perturbation $\Delta\varepsilon$. Finally, as expected, *iv)* for decreasing index contrast, the longitudinal components drop, thus reducing their overall contribution and *quasi-TE* and the *quasi-TM* coupling characteristics tend to have identical behavior.

These results show how one should pragmatically use the CMT to successfully model all kind of devices, ranging from high index contrast and compact ones, such as Silicon or other semiconductor integrated optical devices, down to those with lower index contrast and large footprints.

REFERENCES

1. S. A. Schelkunoff, “Conversion of Maxwell’s equations into generalized telegraphist’s equations”, Bell Syst. Tech. J. **34**, 995–1043 (1955).
2. A. W. Snyder, “Coupled-Mode Theory for Optical Fibers”, J. Opt. Soc. Am. **62**, 1267–1277 (1972).
3. H. Kogelnik, “Theory of dielectric waveguides”, in *Integrated optics*, T. Tamir Ed., New York, Springer-Verlag, 1979, 2nd ed., Chapter 2.
4. A. Yariv, “Coupled-mode theory for guided-wave optics”, IEEE J. Quantum Electronics **QE-9**, pp. 919–933, 1973.
5. D. Marcuse, *Light transmission optics*, 2nd Ed., Van Nostrand Reinhold Company, 1982.
6. A. Hardy and W. Streifer, “Coupled mode theory of parallel waveguides”, IEEE J. Lightwave Technol. **LT-3**, 1135–1146 (1985).
7. E. A. J. Marcatili, “Improved coupled-mode equations for dielectric guides”, IEEE J. Quantum Electronics **QE-22**, 988–993 (1986).
8. H. A. Haus, W. P. Huang, S. Kawakami and N. A. Whitaker, “Coupled-mode theory of optical waveguides”, IEEE J. Lightwave Technol. **LT-5**, 6–23 (1987).
9. S.-L. Chuang, “A Coupled Mode Formulation by Reciprocity and a Variational Principle”, IEEE J. Lightwave Technol. **LT-5**, 5–15 (1987).
10. S.-L. Chuang, “Application of the Strongly Coupled-Mode Theory to Integrated Optical Devices”, IEEE J. Quantum Electronics **QE-23**, 499–509 (1987).
11. W. Streifer, M. Osisnsky and A. Hardy, “Reformulation of the coupled-mode theory of multiwaveguide systems”, IEEE J. Lightwave Technol. **5**, 1–4 (1987).
12. R. G. Peall and R. R. A. Syms, “Comparison between strong coupling theory and experiment for three-arm directional couplers in Ti:LiNbO$_3$”, IEEE J. Lightwave Technol. **7**, 540–554 (1989).
13. D. Marcuse, *Theory of dielectric optical waveguides*, 2nd Ed., Academic Press, 1991.
14. W. Huang, “Coupled-mode theory for optical waveguides: an overview”, J. Opt. Soc. Am. A **11**, 963–983 (1994).
15. B. E. Little and W. P. Huang, “Coupled-Mode Theory for Optical waveguides”, Progress in Electron. Research, PIER 10, 217–270 (1995).
16. S. Yang, M. L. Cooper, P. R. Bandaru, and S. Mookherjea, "Giant birefringence in multi-slotted silicon nanophotonic waveguides," Opt. Express **16**, 8306–8316 (2008).
17. M. L. Cooper and S. Mookherjea, “Numerically-assisted coupled-mode theory for silicon waveguide couplers and arrayed waveguides”, Opt. Express **17**, 1583–1599 (2009).
18. N. Kohli, S. Srivastava and E. K. Sharma, “Orthogonal solutions for asymmetric strongly coupled waveguide arrays: an elegant, analytical approach”, J. Opt. Soc. Am. B **31**, 2871–2878 (2014).

19. N. Kohli, S. Srivastava and E. K. Sharma, “Scalar coupled mode theory and variational analysis for planar SOI waveguide arrays: a detailed comparison”, Optical and Quantum Electronics **48**, 265 (2016).
20. A. Macho, M. Morant and R. Llorente, “Unified model of linear and nonlinear crosstalk in multi-core fiber”, IEEE J. Lightwave Technol. **34**, 3035–3046 (2016).
21. J. Xu and Y. Chen, “General coupled mode theory in non-Hermitian waveguides”, Opt. Express, **23**, 22619–22627 (2015).
22. B. Zhu, G. Ren, Y. Gao, B. Wu, Q. Wang, C. Wan and S. Jian, “Graphene plasmons isolator based on non-reciprocal coupling”, Opt. Express, **23**, 16071–16083 (2015).
23. J. Zhou and P. Gallion, “Comprehensive analytical model to characterize randomness in optical waveguides”, Opt. Express, **24**, 6825–6842 (2016).
24. F. Fogli, N. Greco, P. Bassi, G. Bellanca, P. Aschieri and P. Baldi, “Spatial harmonics modelling of planar periodic segmented waveguides”, Optical and Quantum Electronics **33**, 485–498 (2001).
25. COMSOL Multiphysics software, http://www.comsol.com.
26. L. Szostkiewicz, M. Napierala, A. Ziolowicz, A. Pytel, T. Tenderenda and T. Nasilowski, “Cross talk analysis in multicore optical fibers by supermode theory”, Opt. Lett. **41**, 3759–3762 (2016).
27. R. G. Hunsperger, *Integrated Optics*, 5th Ed, Springer, 2013, Chapt. 8.
28. P. Orlandi, F. Morichetti, M. Strain, M. Sorel, A. Melloni and P. Bassi, “Tunable silicon photonics directional coupler driven by a transverse temperature gradient”, Opt. Lett. **38**, 863–865 (2013).
29. P. Orlandi, F. Morichetti, M. Strain, M. Sorel, P. Bassi and A. Melloni, “Photonic Integrated Filter With Widely Tunable Bandwidth”, IEEE J. Lightwave Technol. **32**, 897–907 (2014).